Article:
Ramesh, K, Smith, AK, Garcia, RR et al. (2020) Long-Term Variability and Tendencies in Migrating Diurnal Tide From WACCM6 Simulations During 1850–2014. Journal of Geophysical Research: Atmospheres, 125 (23). e2020JD033644. ISSN: 2169-897X

https://doi.org/10.1029/2020jd033644

Ramesh Karanam (Orcid ID: 0000-0001-5642-8864)
Smith Anne, K. (Orcid ID: 0000-0003-2384-5033)
Garcia Rolando, R. (Orcid ID: 0000-0002-6963-4592)
Marsh Daniel, R. (Orcid ID: 0000-0001-6699-494X)
Sridharan S (Orcid ID: 0000-0002-0327-3085)
Kishore Kumar Karanam (Orcid ID: 0000-0001-6202-8760)

Long-Term Variability and Tendencies in Migrating Diurnal Tide from WACCM6 Simulations during 1850-2014

K. Ramesh [1,2,*], Anne K. Smith [1], Rolando R. Garcia [1], Daniel R. Marsh [1,3], S. Sridharan [4], K. Kishore Kumar [5]

[1]Atmospheric Chemistry Observations and Modeling (ACOM) Laboratory, National Center for Atmospheric Research (NCAR), Boulder, CO, USA

[2]University Corporation for Atmospheric Research (UCAR), Boulder, CO, USA

[3]University of Leeds, Leeds, UK

[4]National Atmospheric Research Laboratory (NARL), Gadanki, A.P., India

[5]Space Physics Laboratory, Vikram Sarabhai Space Centre (VSSC), Trivandrum, Kerala, India

***Correspondence to**

Karanam Ramesh,

Email: karanamram@gmail.com, kramesh@ucar.edu

Keywords

Atmospheric tides, Mesosphere, Lower stratosphere, Trends

Key points

i. Long-term trends exist in DW1 amplitudes in WACCM6 simulations.

ii. The results suggest that increasing trends in CO_2 as well as ENSO are responsible for the increasing trend in tidal amplitudes.

iii. In addition to CO_2, the global tidal amplitudes in temperature are affected by changes in ODSs in the upper stratosphere.

Abstract

Long-term variability and tendencies in migrating diurnal tide (DW1) are investigated for the first time using a three-member ensemble of historical simulations by NCAR's Whole Atmosphere Community Climate Model, latest version 6 (WACCM6) for 1850-2014 (165 years). The model reproduces the climatological features of the tide in temperature (T), zonal wind (U) and meridional wind (V). The amplitudes peak in the upper mesosphere and lower thermosphere (above ~0.001 hPa) at the equator for T (~10 K) and over 20-30°N and S latitudes for U (~15 m/s) and V (~25 m/s). The contributions of solar cycle (SC), quasi biennial oscillation (QBO) at 10 hPa and 30 hPa, El Niño–southern oscillation (ENSO), ozone depleting substances (ODS), carbon dioxide (CO_2), and stratospheric sulfate aerosols (volcanic eruptions) to change in annual mean amplitudes are analyzed using multiple linear regression. The tidal amplitudes in three components show a long-term increase in the upper stratosphere (0.95 hPa – 10.7 hPa) and the upper mesosphere (0.0001 hPa – 0.01 hPa), predominantly due to increasing CO_2 with a smaller contribution from the trend in ENSO. Interestingly, the global mean tidal amplitude in T decreases sharply after 1950-1960 until 1995 and then increases in association with changes in ODSs. The seasonal differences in tidal responses to the above indices can be as large as the overall signals. All the responses are stronger in the upper mesosphere; however there is also a pronounced negative response

of temperature tide to ODSs over mid-high latitudes around the stratopause (~1 hPa) during all seasons.

1. Introduction

Atmospheric solar tides play a vital role in transferring energy and momentum between various regions of the atmosphere. These global scale oscillations can be observed in temperature, wind, density and pressure. Tides are classified into migrating and non-migrating [*Chapman and Lindzen*, 1970]. Migrating tides are sun-synchronous and follow the apparent westward motion of the sun at periods which are harmonics of a solar day. The dominant dynamical mode in the mesosphere and lower thermosphere (MLT) is the migrating diurnal tide (DW1) [*Chapman and Lindzen*, 1970; *Burrage et al*., 1995]. It is driven primarily by diurnal variations of the solar heating due to the absorption of infrared (IR) radiation by water vapour in the troposphere (~0-15 km) and ultraviolet (UV) radiation by ozone in the stratosphere and lower mesosphere (~30-60 km) [*Forbes*, 1995]. The release of latent heat by deep convection in the tropical troposphere is another excitation mechanism [e.g., *Hagan and Forbes*, 2002; *Chang et al*., 2008; *Mukhtarov et al*., 2009 and references therein; *Davis et al*., 2013]. The tidal perturbations generated in the lower and middle atmosphere propagate vertically with increasing amplitude in response to decreasing density and deposit energy and momentum into the background atmosphere as they dissipate in the MLT region.

Tides continue to be a major focus of scientific research, not only because of their large amplitudes but also due to lack of comprehensive understanding of their short- and long-term variability. Numerous observational and modeling studies have shown that the DW1 amplitude has a strong semi-annual seasonal cycle with maxima during or shortly after equinoxes [e.g. *Burrage et al*., 1995; *Chang et al*., 2008; *Xu et al*., 2009; *Mukhtarov et al*.,

2009; *Smith*, 2012]. Interannual variations that are in phase with the quasi-biennial oscillation (QBO) [e.g., *Xu et al*., 2009] and El Niño–Southern Oscillation (ENSO) [*Gurubaran et al*., 2005; *Lieberman et al*., 2007; *Pedatella and Liu*, 2012] have also been documented. The QBO is an oscillation in the equatorial stratospheric winds between eastward and westward flow, with the phases descending with time, and having a period of ~27 months [e.g., *Reed et al*.,1961]. The QBO is believed to be due to the momentum deposited by upward propagating tropical waves including gravity waves and planetary waves [e.g., *Baldwin and Dunkerton*, 2001]. The tidal propagation into the MLT region depends on wave sources/forcing, wave propagation through background mean zonal winds, and dissipative characteristics, with the QBO affecting tidal propagation. The experimental studies by *Vincent et al*. [1998] reported a March/April maximum of diurnal tidal amplitude when the QBO winds at 30 hPa were eastward. *Gurubaran and Rajaram*, [1999] emphasized the connection between interannual variability in the mesospheric tidal amplitudes and the stratospheric QBO from the long-term MF radar wind observations over Tirunelveli (8.7°N, 77.8 °E). ENSO is a coupled atmosphere and ocean phenomenon connected to irregularly periodic (2-7 years) warming in sea surface temperatures over the equatorial eastern and central eastern Pacific Ocean [e.g., *Gurubaran et al*., 2005]. More details on ENSO can be found in *Scaife et al*., [2019]. It influences the global rainfall, temperature, and wind patterns. The atmospheric response to ENSO involves perturbations in tropospheric convection that influence the tidal forcing and produce large variability in tidal amplitudes in the MLT.

Most of the studies on tides have focused on seasonal, intraseasonal and interannual variability of the DW1 tide using relatively short-term observations and model simulations. Knowledge of how natural forcings such as the solar cycle (SC), QBO, ENSO and long-term changes in radiatively active gases (CO_2, O_3, CH_4, N_2O, chlorofluorocarbons) together affect

the tidal amplitude is scarce. Although some studies have reported a link between the tidal variability and one or more of the above natural forcings [e.g., *Vincent et al*., 1998; *Gurubaran and Rajaram*, 1999; *Hagan et al*., 1999; *Trenberth et al*., 2002; *Gurubaran et al*., 2005, 2009; *Lieberman et al*., 2007; *Xu et al*., 2009; *Sridharan et al*., 2010; *Oberheide et al*., 2011; *Pedatella and Liu*, 2012; *Liu et al*., 2017; *Dhadly et al*., 2018; *Vitharana et al*., 2019; *Sridharan,* 2019, 2020], they focus either on short periods or on a specific geographic location. Furthermore none of these studies have looked at all of the different forcings combined.

The present study provides the first detailed investigation of the variability and long-term tendencies of the DW1 amplitudes in middle atmosphere (stratosphere and mesosphere) since preindustrial times (1850-1860) associated with solar activity, QBO, ENSO, ozone depleting substances (ODS), carbon dioxide (CO_2), and stratospheric sulfate aerosols (produced primarily by volcanic eruptions). The results are based on an ensemble of three realizations with historical simulations of NCAR's Whole Atmosphere Community Climate Model version 6 (WACCM6) for the period of 1850-2014 (165 years). Here realizations stand for model runs starting on the same calendar date but with different initial conditions, as discussed in Section 2.1. The long-term variability and tendencies are derived with respect to the pre-industrial time of 1850-1860 using multiple linear regression (MLR) analysis. Section 2 provides the brief description of model simulations and data analysis, section 3 presents the results, section 4 discusses the results and concluding remarks are provided in section 5.

2. Model Simulations and Methodology

2.1. WACCM6 Description

WACCM is a comprehensive global climate numerical model that extends from Earth's surface into the lower thermosphere ($6x10^{-6}$ hPa; ~140 km). The latest version, WACCM6 [*Gettleman et al*., 2019] is run as the atmospheric component of NCAR's Community Earth System Model, version 2 (CESM2) [*Danabasoglu et al*., 2020]. It simulates a self-generated QBO and ENSO with realistic magnitude and occurrence rate. The vertical resolution changes with altitude from 1.1 - 1.4 km in the troposphere and lower stratosphere to 1.75 km in the upper stratosphere and 3.5 km in the upper mesosphere and lower thermosphere [*Garcia et al*, 2017]. The changes to this version from the previous release (WACCM4; *Marsh et al*., 2013) include higher horizontal resolution of 0.95°x1.25° (latitude x longitude) and additional chemical compounds and reactions, including additions to the representation of ion chemistry and heterogeneous reactions. An extensive description of WACCM6, including several important features of the model and its validation, can be obtained from *Gettelman et al*., [2019]. In the configuration used in this investigation, the atmospheric model includes coupled chemistry and a coupled ocean model.

The diurnal tides in WACCM6 are computed using every model timestep (30-minute resolution) and archived as monthly means. In the present investigation, we compute monthly mean amplitudes of the migrating diurnal tide in temperature (T_{24}), zonal wind (U_{24}) and meridional wind (V_{24}) to investigate the long-term variability and the response to the SC, QBO, ENSO, ODSs, CO_2 and stratospheric sulfate aerosols in the middle atmosphere and lower thermosphere during 1850-2014 from three realizations. The three realizations were started from an energy-balanced pre-industrial Control simulation, at times separated by 5 to 10 years, such that ENSO, QBO and other atmospheric and ocean cycles are in different

states at the start of each realization. As a result, the internal dynamical variability in the three realizations is largely uncorrelated, which facilitates isolation of the responses to external forcing.

2.2. Methodology

The dependency of tidal amplitude on the seven indices (there are two indices for the QBO) is derived from MLR analysis. The regression model uses monthly output averaged either over 12 months, for year-to-year variations, or over three months of each year for seasonal variations. The analysis is carried out for the period 1850-2014 at each latitude and pressure grid point with anomalies with respect to 1850-1860. The expression for MLR model is given below.

$$\alpha(t) = K + C_1.F_{10.7} + C_2.QBO10 + C_3.QBO30 + C_4.NINO3.4 + C_5.EESC + C_6.CO_2 + C_7.AOD + \varepsilon(t)$$

…….. (1)

where α is the predictand (T_{24} or U_{24} or V_{24}), t is time (years), K is a constant, C_1-C_7 are regression coefficients and ε is the residual. All the predictors are defined from the three realizations of WACCM6. $F_{10.7}$ is the solar radio flux at 10.7 cm, a proxy for solar activity (in solar flux unit, sfu; 1 sfu=10^{-22} Wm^{-2} Hz^{-1}); for *QBO10* and *QBO30,* the zonal wind (ms^{-1}) is averaged over 5°N-5°S at 10 hPa and 30 hPa, respectively; the *NINO3.4* index is the 3-month running mean of sea surface temperature (K) averaged for 5°N-5°S and 120°W-170°W; *EESC* (Equivalent Effective Stratospheric Chlorine in ppbv) is proxy for ODS and calculated as the area-weighted global average of the sum of the inorganic chlorine and 60 times the inorganic bromine (ClO_y+60 BrO_y) at 1 hPa pressure. Here the number 60 signifies that bromine is 60 times more efficient than chlorine in destroying ozone [*Newman et al*., 2007; *Stolarski et al*., 2010]. The CO_2 represents the global mean of surface carbon dioxide

volume mixing ratio (ppmv) and *AOD* is area weighted global mean of stratospheric aerosol optical depth at 550 nm as proxy for stratospheric sulfate aerosols (volcanic eruptions). The $F_{10.7}$ radio flux index and the global mean surface CO_2 are specified in the model simulations. The other indices are calculated from the model chemical or dynamical fields.

The seasonal and annual predictors are defined as the anomalies with respect to the pre-industrial period of 1850-1860. The regression coefficients/responses and the contributions (product of regression coefficient and the corresponding index) to the simulated changes are calculated for three realizations separately and then averaged for presentation.

3. Results

In this section, we present first the overall picture (latitude-pressure) of DW1 tidal variability in four seasons from WACCM6 simulations and then the predictors defined for MLR analysis along with their temporal variations. Also, the changes in tidal amplitudes (ΔT_{24}, ΔU_{24}, ΔV_{24}) from the pre-industrial time (1850-1860) and the responses/contributions of the natural and anthropogenic forcings are presented.

3.1. Seasonal and Latitudinal Variation of DW1 Amplitude

Figure 1 shows the latitude-pressure variation of composite mean (averaged for 1850-2014 over the three realizations) DW1 amplitudes in T, U and V for four seasons: MAM (March, April, May), JJA (June, July, August), SON (September, October, November) and DJF (December, January, February). The maximum amplitudes occur in the upper mesosphere and lower thermosphere (above ~0.01 hPa) over the equator in T_{24} (up to 10 K) and around 20-30°N and S in U_{24} (up to 15 m/s) and V_{24} (up to 25 m/s). The local maxima in T_{24} around the stratopause (~1 hPa) over mid-high latitudes are consistent with the first

symmetric trapped (1, -2) mode [*Pancheva and Mukhtarov*, 2011], which does not propagate vertically into the mesosphere. The amplitudes in the three components are larger in MAM and DJF and this variation is comparatively stronger in V_{24} than in U_{24}. The seasonal behaviour of the simulated tide differs somewhat from numerous observations indicating maxima at the equinoxes.

3.2. Time Series of the Predictors

The time series of the annual mean predictors used for the regression analysis are shown in **Figure 2** for 1850-2014. Four of the predictors, viz., $F_{10.7}$, EESC, CO_2 and AOD, are identical, or almost identical, in the three realizations. The QBO10, QBO30 and NINO3.4 are uncorrelated among the three realizations. There are no apparent long-term trends in the QBO indices. There is a trend in the NINO3.4 index in the most recent decades that is consistent with an overall warming in the ocean temperature. More details on the predictors can be obtained from *Ramesh et al*., [2020].

3.3. Temporal Variation of Annual Mean Tide

The left column of **Figure 3** shows the upper stratosphere (0.95 hPa - 10.7 hPa; ~30.4 km – 48.3 km) annual mean of ΔT_{24} (left y-axis), ΔU_{24} and ΔV_{24} (right y-axis) along with the contributions due to the seven predictors for the latitudes where the tidal fields peak (T_{24} at the equator; U_{24} and V_{24} averaged over 20-30°N and S; this average is denoted as E23 hereafter). Δ refers to difference since 1850-1860. The ΔT_{24}, ΔU_{24} and ΔV_{24} are further compared with that of the area-weighted global average of each field given in the right column. The regression coefficients from the MLR analysis are significant at the 95% confidence level (significance level is 0.05) for each realization for E23 and global averages. The tidal amplitude increases with time for E23 in all three components; the increase is

slower before 1950 and accelerates afterwards. The global U_{24} and V_{24} also increase but at a relatively slower rate after this year. It is worth noting that the global T_{24} (top right panel of Figure 3) increases until 1950-1960 but drops sharply afterwards, until the late 2000's, when it increases again. This difference between T_{24} and the wind tides appears in the global mean but not at the equator (top left panel) and is confined to the pressure range encompassing the stratopause (cf. Fig. 4, top row). These characteristics suggest that the different behavior of E23 vs. global mean amplitude may be related to the effects of superposition of tidal modes near the stratopause. It is well known [*Chapman and Lindzen*, 1970] that the tidal response near the stratopause consists of the superposition of a vertically-propagating component, approximated by the (1,1) Hough mode, which is forced by heating due to water vapor in the troposphere, and a non-propagating component, forced in situ by ozone heating. The former is narrow in latitude, whereas the latter is very broad (and would be expected to dominate the response in the global mean, but not in E23). Insofar as the global mean T_{24} decreases and increases in unison with the behavior of EESC (cf. Fig. 3, first and sixth rows of the right column), the reduced amplitude of global mean T_{24} during the period of fast EESC growth is likely to be due to the reduction of ozone (and the concomitant reduction of heating; see *Garcia et al*., [2019]) at this time.

We discuss the responses to each of the predictors in the order shown in Figure 3 (top to bottom). Note that the units are the same in each panel so the magnitudes can be directly compared. The influence of solar cycle is clearly noticed in all three components of the tide although it is very small. This could be due to the fact that the solar flux at the wavelengths responsible for heating near 1 hPa does not have a large SC variation. The magnitude is relatively smaller in U_{24} than in V_{24}. It is interesting that the U_{24} response to $F_{10.7}$ is substantially stronger in the global mean than at averages for 20-30° N and S. It could be due

to the average over 20-30° N and S does not capture all of the U_{24} maxima (note that U_{24} has large amplitude beyond 20-30° latitudes, especially at the solstices, as per Fig. 1). The annual mean QBO and NINO3.4 signals are also quite small; the latter exhibits an increasing trend that is more pronounced after 1950. The magnitude of the equivalent effective stratospheric chlorine (EESC) contribution increases abruptly after 1950; the signals in global mean T_{24} and in U_{24}, V_{24} over both E23 and global mean are negative while that for T_{24} at the equator is positive. The EESC signals in all three tidal components begin to change after 1995. The regression analysis attributes the long-term increase in DW1 amplitude mainly to increasing trend in CO_2. However, as shown in *Ramesh et al*. [2020], a complete separation of trends due to CO_2 and EESC is not possible because of similarities in the time series of forcing. Although the stratospheric aerosols (AOD) have negligible impact on global mean tidal amplitudes, they show negative contribution in all the three components for E23 with slightly larger effect on U_{24} than V_{24}.

Figure 4 is similar to the Figure 3 except for a pressure range in the upper mesosphere lower thermosphere (0.0001 hPa - 0.01 hPa; ~79 km – 107 km). T_{24}, U_{24}, and V_{24} increase in this region also. The trends and the contributions of the predictors are similar for the global mean and E23 except for the contribution of the solar cycle. For E23, the solar contribution to T_{24} is out of phase with those in U_{24} and V_{24}; i.e., when the solar flux is higher, the amplitude of T_{24} is higher but the amplitudes of U_{24} and V_{24} are lower. This could be related to in-situ contributions to the DW1 temperature amplitudes versus increased dissipation of DW1 wind amplitudes at solar minimum versus solar maximum. The QBO signals show appreciable year-to-year variability but no long-term trend. The amplitude response to EESC is negative and its contribution to the overall trend has a magnitude of about 10% of that from CO_2. CO_2 is the dominant contributor to the increasing trend in the

tidal amplitude.

3.4. Latitudinal Distribution of the Responses

Figure 5 illustrates the latitude-pressure variation of the ΔT_{24} response to the seven predictors in four seasons. Note that the units are defined differently for each row; in this figure we want to emphasize the seasonal responses to each predictor rather than the comparisons between the responses to the various predictors. The statistical significance of the responses is calculated from t-test [e.g., *Wilks*, 2006] and the regions where the results are not significant at the 95% confidence level are denoted by stippling in the figures. It is clear that the responses vary quite a bit among seasons although some common features are seen. The magnitudes peak in the equatorial upper mesosphere in all seasons for all the predictors except $F_{10.7}$. The response due to the solar cycle is positive and peaks at and above the mesopause (~0.0003 hPa, ~100 km) globally; this distribution could be due to the in-situ generated DW1 tide in the thermosphere. It is worth noting that the EESC signal is negative around the stratopause in all seasons over mid-high latitudes and has a significantly strong response in the summer hemisphere. The meridionally broad tidal responses at the stratopause are characteristic of trapped tidal modes that are generated in situ due to the solar heating from stratospheric ozone. The negative ΔT_{24} response to EESC is associated with declining ozone concentration. There is also a negative signal in the summer mesosphere that has a latitude and pressure structure indicative of the dominant diurnal tide.

Figure 6 is similar to Figure 5, but for ΔV_{24}. The ΔU_{24} responses (not shown) are very similar to, although weaker than, those of ΔV_{24}. The statistically significant responses due to all the predictors except for $F_{10.7}$ are largely confined to 15-30°N and S and peak in the upper mesosphere. Some of the responses ($F_{10.7}$, NINO3.4, EESC and AOD) are variable in sign

and not significant.

4. Discussion

The simulations indicate long-term increase in tidal amplitudes in the upper stratosphere and upper mesosphere. The analysis indicates that the three variables that are most important in predicting long-term changes in tidal amplitude are CO_2 concentration, EESC, and solar variability. Increasing CO_2 enhances the solar heating through its effect of increasing water vapor in the troposphere. The analysis indicates that there is a secondary contribution (with smaller values than the contribution due to CO_2) from the trend in ENSO (NINO3.4), which influences tropical convection and latent heat release.

As seen in Figure 3, the global mean T_{24} in the upper stratosphere decreases abruptly after 1950-1960 and then starts to increase around 1995. The DW1 tide is partially forced by the direct absorption of solar radiation by ozone in the stratosphere. The extratropical diurnal temperature variation near the stratopause is trapped; i.e. it is locally forced but does not propagate vertically. The coincidence in the timing of the extratropical T_{24} changes and the increase in ODSs (EESC) suggests a mechanism. The decrease in ozone abundance due to photochemical loss during 1950-1995 in turn reduces solar heating and thereby reduces that part of the diurnal variation in temperature in the upper stratosphere that is forced in situ by solar heating. Such a change in the diurnal temperature variation will be seen as a reduction in T_{24} even when it is not a propagating tide. The fact that similar changes are not seen is U_{24} and V_{24} supports this interpretation. Afterward, the recovery of ozone due to declining ODSs reverses this trend.

In contrast, both the overall change in T_{24} (top left panel of Figure 3) and the EESC contribution to it show positive responses over the equator. This suggests that T_{24} at the equator is not dominated by the trapped mode, which leads in turn to the conclusion that the propagating tide has larger amplitude than the trapped tide there. As shown in *Ramesh et al.* [2020], the MLR analysis cannot cleanly separate the responses to forcing from CO_2 and from ODS. The low latitude responses of T_{24}, U_{24}, and V_{24} to ODS appear to be contradictory, suggesting that a decrease in ozone concentration leads to a larger tide. It is plausible that this positive response of DW1 to ODS is another indication of the ambiguity of sorting out which mechanisms are forcing long-term variations in the stratosphere. Another plausible explanation is that the tide forced by ozone heating is out of phase with that propagating from the troposphere so that they destructively interfere. In that case, a decrease in ozone heating would amplify the net tidal amplitude; evaluation of this option requires additional diagnostic information not available from the WACCM simulations. An impact of EESC on the propagating tide would be identifiable in the region above the stratopause. There, the signal is not clear. T_{24} over the equator (Figure 5) shows a variable response: positive in some seasons, negative in others. The most coherent negative response is seen during JJA (Figures 5 and 6), when the T_{24} is weakest (Figure 1).

The response of ozone in the tropical upper stratosphere to the solar cycle is positive [e.g., *Nath and Sridharan*, 2014; *Ball et al*., 2019]. Due to the solar heating from ozone SW absorption [e.g., *Hagan*, 1996; *McLandress*, 1997], which maximizes in the upper stratosphere, the ΔT_{24} is in phase with the solar cycle up to upper mesosphere. However, the ΔU_{24} and ΔV_{24} over 20-30° latitudes in both hemispheres are in phase with solar cycle in the upper stratosphere but out of phase in the upper mesosphere. *Sridharan et al*. [2010] observed a negative response of the diurnal tide in wind fields (U,V) over Tirunelveli (8.7°N, 77.8°E)

in the upper mesosphere above ~80 km. *Singh and Gurubaran*, [2017] presented the anticorrelation between V_{24} and the sunspot number (SSN). The consistency in sign in the response to solar variability between the analysis of WACCM results presented here and the observations cited above gives confidence that the simulated response is realistic.

5. Conclusions

The important conclusions drawn from this study can be summarized as follows.

i. The historical simulations show the long-term increase in annual mean tidal amplitudes in temperature (except global mean in upper stratosphere) and horizontal winds largely through increasing CO_2 while the trend in ENSO plays secondary role.

ii. The global temperature amplitude decreases sharply after 1950-1960 until 1995 and then increases in association with changes in ODSs.

iii. The tidal amplitudes are positively correlated with SC in all three components, however in the upper mesosphere, the wind amplitudes are anticorrelated with SC over 20-30° latitudes.

iv. The latitude-pressure distributions of responses indicate that the variations mostly peak at the latitudes and pressures where the tidal amplitudes themselves peak. An exception is the strong negative response of T_{24} to EESC around the stratopause at mid-high latitudes in association with the trapped modes.

6. Acknowledgments

This research is supported by the NASA Living With a Star (LWS) Jack Eddy Postdoctoral Fellowship Program, administered by UCAR's Cooperative Programs for the Advancement of Earth System Science (CPAESS) under award #NNX16AK22G. One of the authors (K. Ramesh) is thankful to UCAR and NASA for the support through above

fellowship. The authors are grateful to Nicholas Pedatella and Federico Gasperini of HAO for their helpful comments and suggestions on the original manuscript. The NCAR is sponsored by the National Science Foundation (NSF). The computing and data storage resources including Cheyenne super computer (doi: 10.5065/D6RX99HX) were provided by the Computational and Information Systems Laboratory (CISL) at NCAR. The archived model data used in this study can be obtained from https://esgf-node.llnl.gov/projects/cmip6/. WACCM6 code is available as part of the CESM2 release via github and the instructions are available at: http://www.cesm.ucar.edu/models/cesm2/release_download.html. The authors are thankful to the Editor and the three anonymous reviewers for their constructive comments and suggestions which greatly helped to improvise the manuscript.

7. References

Ball, W. T., E. Rozanov, J.A. Alsing, D.R. Marsh, F. Tummon, D.J. Mortlock et al. (2019), The upper stratospheric solar cycle ozone response, *Geophys. Res. Lett.*, 46, https://doi.org/10.1029/2018GL081501.

Baldwin, M.P., T.J. Dunkerton (2001), Stratospheric harbingers of anomalous weather, *Science*, 294(5542):581-584. doi:10.1126/science.1063315.

Burrage, M.D., M.E. Hagan, W.R. Skinner, D.L. Wu, and P.B. Hays (1995), Long-term variability in the solar diurnal tide observed by HRDI and simulated by the GSWM, *Geophys. Res. Lett.*, 22, 2641-2644, https://doi.org/10.1029/95GL02635.

Chapman, S., and R.S. Lindzen (1970), Atmospheric Tides: Thermal and Gravitational, Gordon and Breach, New York.

Chang, L., S. Palo, M. Hagan, J. Richter, R. Garcia, D. Riggin, and D. Fritts (2008), Structure of the migrating diurnal tide in the Whole Atmosphere Community Model (WACCM), *Adv. Space Res.*, 41(9), 1398-1407.

Dhadly, M. S., Emmert, J. T., Drob, D. P., McCormack, J. P., & Niciejewski, R. (2018), Short-term and interannual variations of migrating diurnal and semidiurnal tides in the mesosphere and lower thermosphere, *J. Geophys. Res. Space Phys*., 123, 7106–7123. https://doi.org/10.1029/2018JA025748.

Danabasoglu, G., J.-F.Lamarque, J. Bacmeister, D.A. Bailey, A.K. DuVivier, J. Edwards, et al. (2020), The Community Earth System Model Version 2 (CESM2). *J. Adv. Modeling Earth Sys*, 12(2), e2019MS001916, https://doi.org/10.1029/2019MS001916.

Davis, R. N., J. Du, A. K. Smith, W. E. Ward, and N. J. Mitchell (2013), The diurnal and semidiurnal tides over Ascension Island (8°S, 14°W) and their interaction with the stratospheric quasi-biennial oscillation: Studies with meteor radar, eCMAM and ACCM, *Atmos. Chem. Phys.*, 13, 9543– 9564, doi:10.5194/acp-13-9543-2013.

Forbes, J. M. (1995), Tidal and planetary waves, in The Upper Mesosphere and Lower Thermosphere: A Review of Experiment and Theory, *Geophys. Monogr*., Ser, vol. 87, edited by R. M. Johnson and T. L. Killeen, pp. 67–87, AGU, Washington, D. C.

Garcia, R. R., A.K. Smith, D.E. Kinnison, Á. de la Cámara, and D.J. Murphy (2017), Modification of the gravity wave parameterization in the Whole Atmosphere Community Climate Model: Motivation and results, *J. Atmos. Sci*., 74, 275–291, https://doi.org/10.1175/JAS-D-16-0104.1.

Garcia, R. R., Yue, J., & Russell, J. M. (2019). Middle atmosphere temperature trends in the twentieth and twenty-first centuries simulated with the Whole Atmosphere Community Climate Model (WACCM), *J. Geophys. Res. Space Phys*., 124, 7984–7993. https://doi.org/10.1029/2019JA026909.

Gettelman, A., Mills, M. J., Kinnison, D. E., Garcia, R. R., Smith, A. K., Marsh, D. R., et al. (2019), The whole atmosphere community climate model version 6 (WACCM6), *J. Geophys. Res. Atmos*, 124, 12380– 12403. https://doi.org/10.1029/2019JD030943.

Gurubaran, S., and R. Rajaram (1999), Long-term variability in the mesospheric tidal winds observed by MF radar over Tirunelveli (8.7°N, 77.8°E), *Geophys. Res. Lett*., 26, 1113– 1116.

Gurubaran, S., R. Rajaram, T. Nakamura, and T. Tsuda (2005), Interannual variability of diurnal tide in the tropical mesopause region: A signature of the El Nino–Southern Oscillation (ENSO), *Geophys. Res. Lett.*, 32, L13805, doi:10.1029/2005GL022928.

Gurubaran, S., R. Rajaram, T. Nakamura, T. Tsuda, D. Riggin, and R.A. Vincent (2009), Radar observations of the diurnal tide in the tropical mesosphere-lower thermosphere region: Longitudinal variabilities. *Earth, Planets and Space*, 61(4), 513–524, https://doi.org/10.1186/BF03353168.

Hagan, M. E., M. D. Burrage, J. M. Forbes, J. Hackney, W. J. Randel, and X. Zhang (1999), GSWM-98: Results for migrating solar tides, *J. Geophys. Res. Space Phys*., 104, 6813–6828.

Hagan, M. E. (1996), Comparative effects of migrating solar sources on tidal signatures in the middle and upper atmosphere, *J. Geophys. Res. Atmos.*, 101(D16), 21213– 21222, doi:10.1029/96JD01374.

Hagan, M. E., and J. M. Forbes (2002), Migrating and nonmigrating diurnal tides in the middle and upper atmosphere excited by tropospheric latent heat release, *J. Geophys. Res. Atmos*, 107 (D24), 4754, doi:10.1029/2001JD001236.

Lieberman, R. S., D.M. Riggin, D.A. Ortland, S.W. Nesbitt and R.A. Vincent (2007), Variability of mesospheric diurnal tides and tropospheric diurnal heating during 1997–1998, *J. Geophys. Res. Atmos.*, 112, D20110, doi:10.1029/2007JD008578.

Liu, H., Sun, Y.-Y., Miyoshi, Y., and H. Jin (2017), ENSO effects on MLT diurnal tides: A 21 year reanalysis data-driven GAIA model simulation, *J. Geophys. Res. Space Physics*, 122, 5539–5549, doi:10.1002/2017JA024011.

Marsh, D.R., M.J. Mills, D.E. Kinnison, J. Lamarque, N. Calvo, and L.M. Polvani, (2013), Climate Change from 1850 to 2005 Simulated in CESM1(WACCM), *J. Climate*, 26, 7372–7391,https://doi.org/10.1175/JCLI-D-12-00558.1.

McLandress, C. (1997), Seasonal variability of the diurnal tide: Results from the Canadian middle atmosphere general circulation model, *J. Geophys. Res. Atmos.*, 102(D25), 29747–29764, doi:10.1029/97JD02645.

Mukhtarov, P., D. Pancheva, and B. Andonov (2009), Global structure and seasonal and interannual variability of the migrating diurnal tide seen in the SABER/TIMED temperatures between 20 and 120 km, *J. Geophys. Res. Space Phys.*, 114, A02309, doi:10.1029/2008JA013759.

Nath, O., and S. Sridharan (2014), Long-term variabilities and tendencies in zonal mean TIMED–SABER ozone and temperature in the middle atmosphere at 10–15°N, *J. Atmos. Sol. Terr. Phys.*, 120, 1-8, https://doi.org/10.1016/j.jastp.2014.08.010.

Newman, P. A., Daniel, J. S., Waugh, D. W., and Nash, E. R., (2007), A new formulation of equivalent effective stratospheric chlorine (EESC), *Atmos. Chem. Phys.*, 7, 4537-4552, https://doi.org/10.5194/acp-7-4537-2007.

Oberheide, J., J.M. Forbes, X. Zhang and S.L. Bruinsma (2011), Climatology of upward propagating diurnal and semidiurnal tides in the thermosphere, *J. Geophys. Res. Space. Phys.*, 116, A11306, doi:10.1029/2011JA016784.

Pancheva D., P. Mukhtarov (2011), Atmospheric Tides and Planetary Waves: Recent Progress Based on SABER/TIMED Temperature Measurements (2002–2007). In: Abdu M.,

Pancheva D. (eds) *Aeronomy of the Earth's Atmosphere and Ionosphere*, IAGA Special Sopron Book Series, vol 2. Springer, Dordrecht.

Pedatella, N. M., and H.-L. Liu, (2012), Tidal variability in the mesosphere and lower thermosphere due to the El Niño–Southern Oscillation, *Geophys. Res. Lett.*, 39, L19802, doi:10.1029/2012GL053383.

Ramesh, K., Anne K. Smith, Rolando R. Garcia, Daniel R. Marsh, Sridharan, S., and Kishore Kumar, K. (2020), Long-Term Variability and Tendencies in Middle Atmosphere Temperature and Zonal Wind from WACCM6 Simulations during 1850-2014, *J. Geophys. Res. Atmos*., (accepted).

Reed, R. J., Campbell, W. J., Rasmussen, L. A., and Rogers, D. G. (1961), Evidence of a downward propagating, annual wind reversal in the equatorial stratosphere, *J. Geophys. Res.*, 66(3), 813– 818, doi:10.1029/JZ066i003p00813.

Scaife, A., Guilyardi, E., Cain, M., Gilbert, A. and the RMetS Climate Science Communications Group(2019), What is the El Niño–Southern Oscillation?. *Weather*, 74: 250-251. doi:10.1002/wea.3404.

Singh, D., and S. Gurubaran (2017), Variability of diurnal tide in the MLT region over Tirunelveli (8.7°N), India: Consistency between ground- and space-based observations, *J. Geophys. Res. Atmos*., 122, 2696–2713, doi:10.1002/2016JD025910.

Smith, A.K. (2012), Global Dynamics of the MLT, *Surv Geophys*, 33, 1177–1230, https://doi.org/10.1007/s10712-012-9196-9.

Sridharan, S., T. Tsuda and S. Gurubaran (2010), Long-term tendencies in the mesosphere/lower thermosphere mean winds and tides as observed by medium-frequency radar at Tirunelveli(8.7°N, 77.8°E), *J. Geophys. Res. Atmos.*, 115, D08109, doi:10.1029/2008JD011609.

Sridharan, S. (2019), Seasonal variations of low-latitude migrating and nonmigrating diurnal and semidiurnal tides in TIMED-SABER temperature and their relationship with source variations, *J. Geophys. Res. Space Physics*, 124, 3558–3572, https://doi.org/10.1029/2018JA026190.

Sridharan, S. (2020), Equatorial upper mesospheric mean winds and tidal response to strong El Niño and La Niña, *J. Atmos. Sol. Terr. Phys*., 202, 1-7, https://doi.org/10.1016/j.jastp.2020.105270.

Stolarski, R.S., A.R. Douglass, P.A. Newman, S. Pawson, and M.R. Schoeberl (2010), Relative Contribution of Greenhouse Gases and Ozone-Depleting Substances to Temperature Trends in the Stratosphere: A Chemistry–Climate Model Study, *J. Climate*, 23, 28–42, https://doi.org/10.1175/2009JCLI2955.1.

Trenberth, K. E., J.M. Caron, D.P. Stepaniak, and S. Worley (2002), Evolution of El Niño–Southern Oscillation and global atmospheric surface temperatures, *J. Geophys. Res.*, 107 (D8), doi:10.1029/2000JD000298.

Vincent, R. A., S. Kovalam, D. C. Fritts, and J. R. Isler (1998), Long-term MF radar observations of solar tides in the low-latitude mesosphere: Interannual variability and comparisons with GSWM, *J. Geophys. Res. Atmos.*, 103, 8667– 8683.

Vitharana, A., Zhu, X., Du, J., Oberheide, J., & Ward, W. E. (2019), Statistical modeling of tidal weather in the mesosphere and lower thermosphere, *J. Geophys. Res. Atmos*., 124, 9011– 9027, https://doi.org/10.1029/2019JD030573.

Wilks, D.S. (2006), *Statistical Methods in the Atmospheric Sciences*, 2nd Edition, Academic Press, San Diego, California.

Xu, J., A. K. Smith, H.-L.Liu, W.Yuan, Q. Wu, G. Jiang, M. G. Mlynczak, J. M. Russell and S. J. Franke, (2009), Seasonal and quasi-biennial variations in the migrating diurnal tide

observed by Thermosphere, Ionosphere, Mesosphere, Energetics and Dynamics (TIMED), *J. Geophys. Res. Atmos.*, 114, D13107, doi:10.1029/2008JD011298.

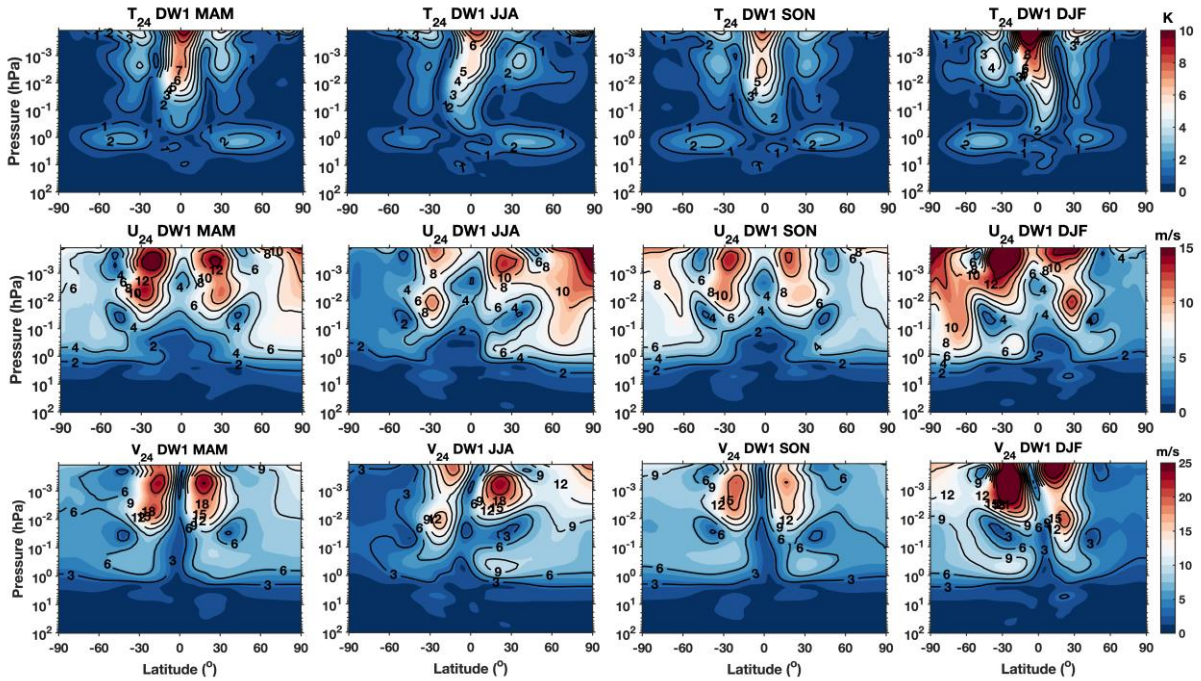

Figure 1. The seasonal and latitude-pressure variation of composite mean (1850-2014) DW1 amplitudes in T, U, V averaged for three realizations. Contour intervals are 1 K for the top panels, 2 m/s for the center panels, and 3 m/s for the bottom panels.

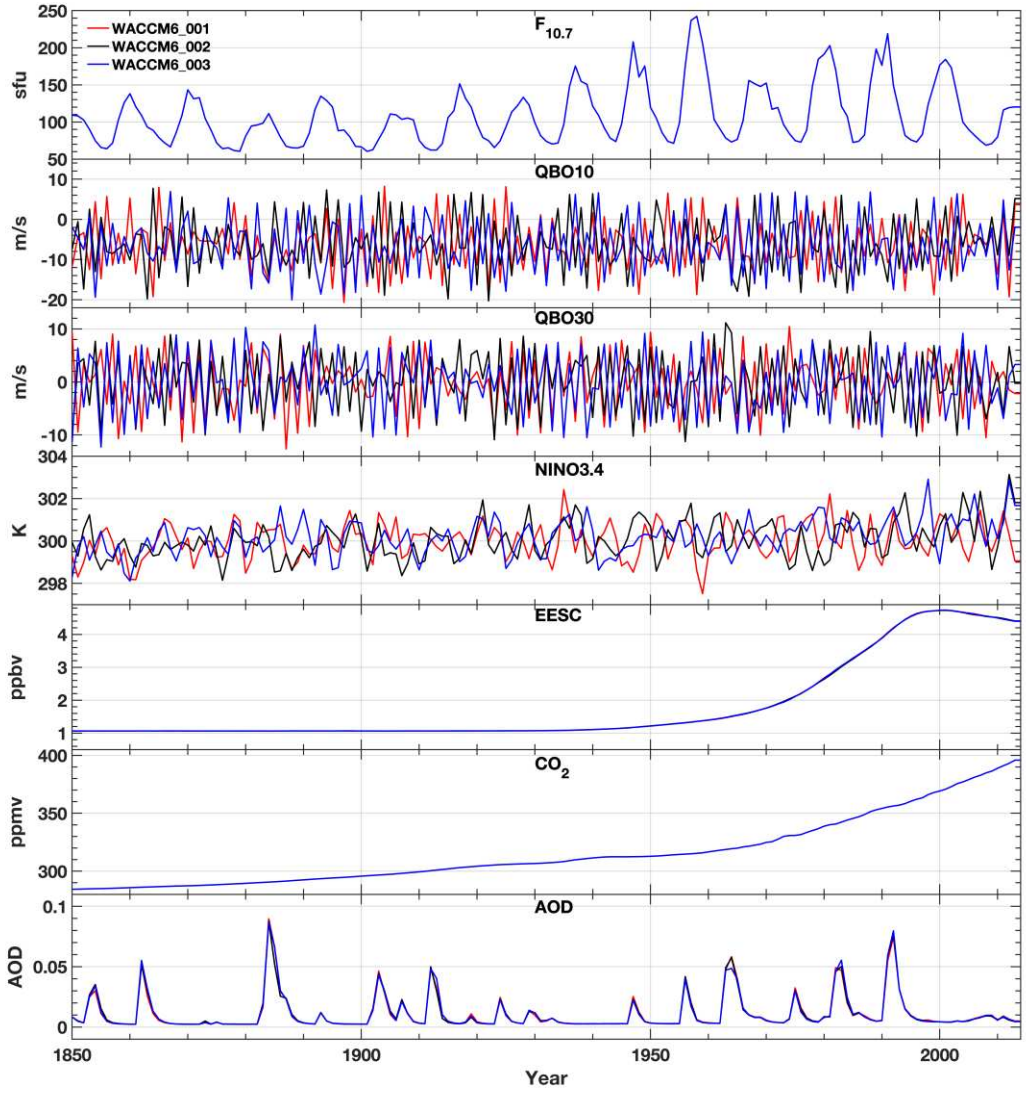

Figure 2. The time series of annual mean of seven predictors for three model realizations during 1850-2014.

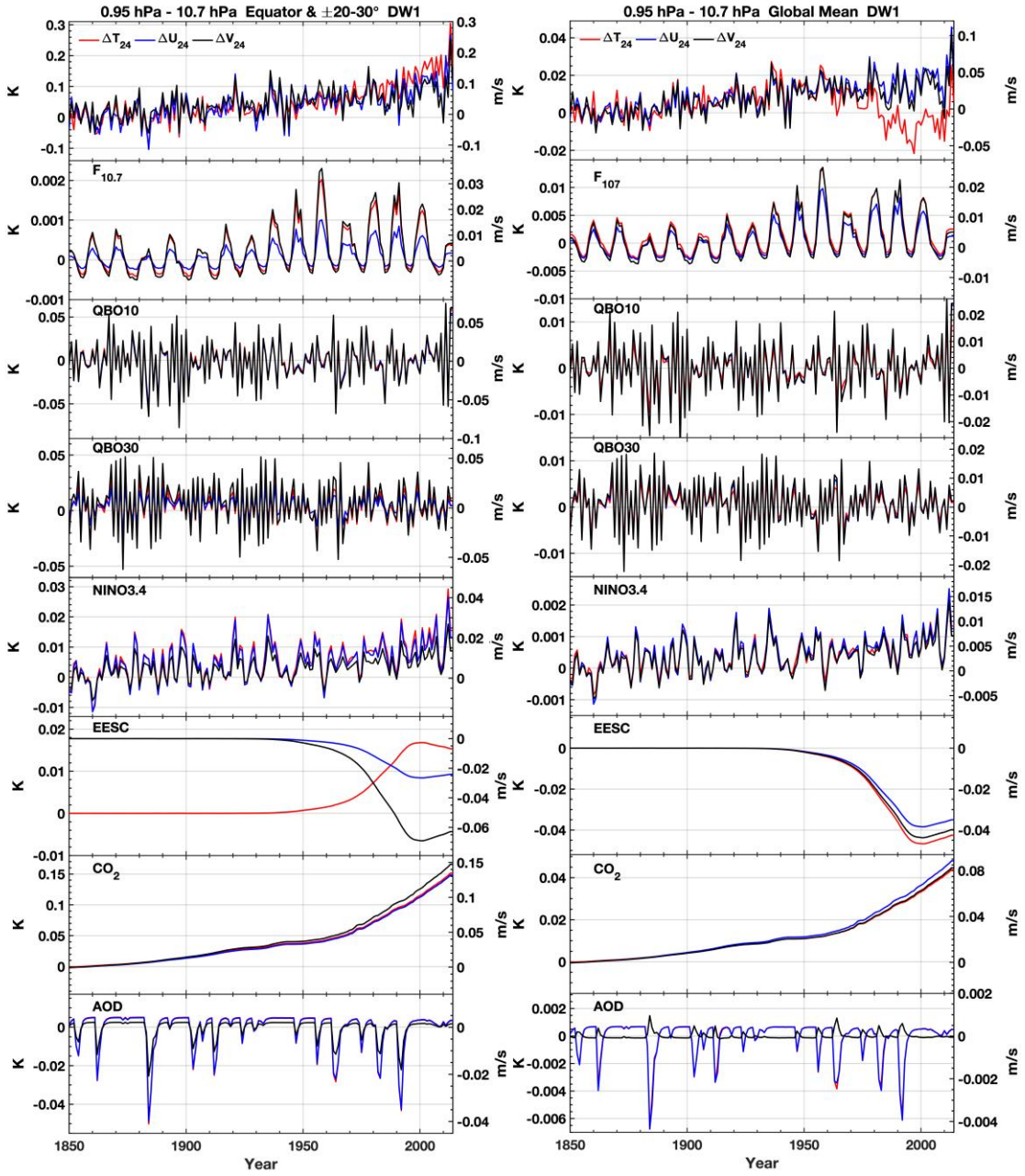

Figure 3. The temporal variation of annual mean and area weighted global mean ΔT_{24}, ΔU_{24}, ΔV_{24} (mean of three realizations) and the contribution of each index viz., $F_{10.7}$, QBO10, QBO30, NINO3.4, EESC, CO_2 and AOD averaged (left panel) at equator for ΔT_{24} and over ±20-30° latitudes for ΔU_{24}, ΔV_{24} and (right panel) globally in the upper stratosphere (0.95 hPa – 10.7 hPa) with ΔT_{24} and its contributions on the left y-axis and for ΔU_{24}, ΔV_{24} on the right y-axis.

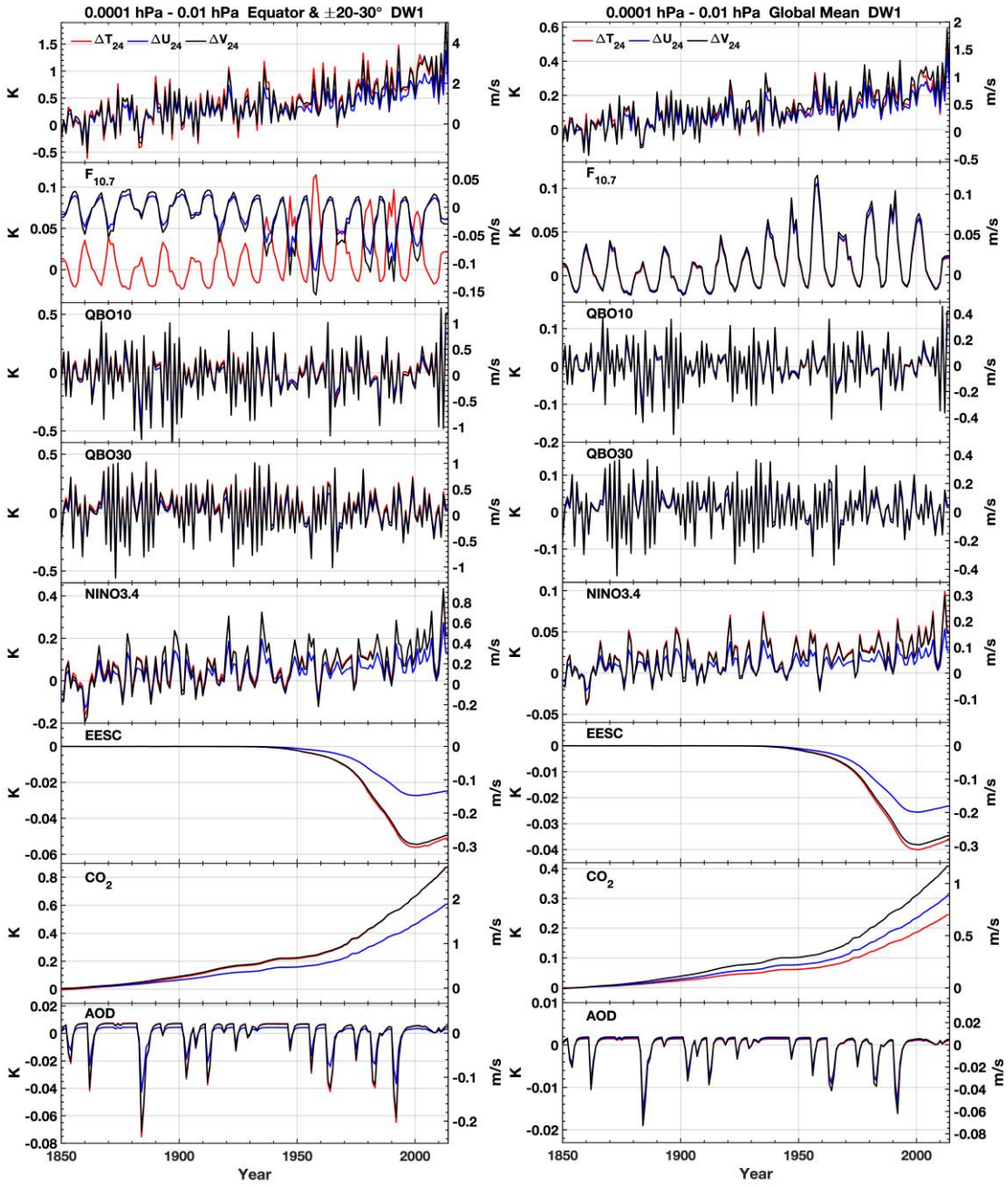

Figure 4. Same as Figure 3 but in the upper mesosphere (0.0001 hPa – 0.01 hPa).

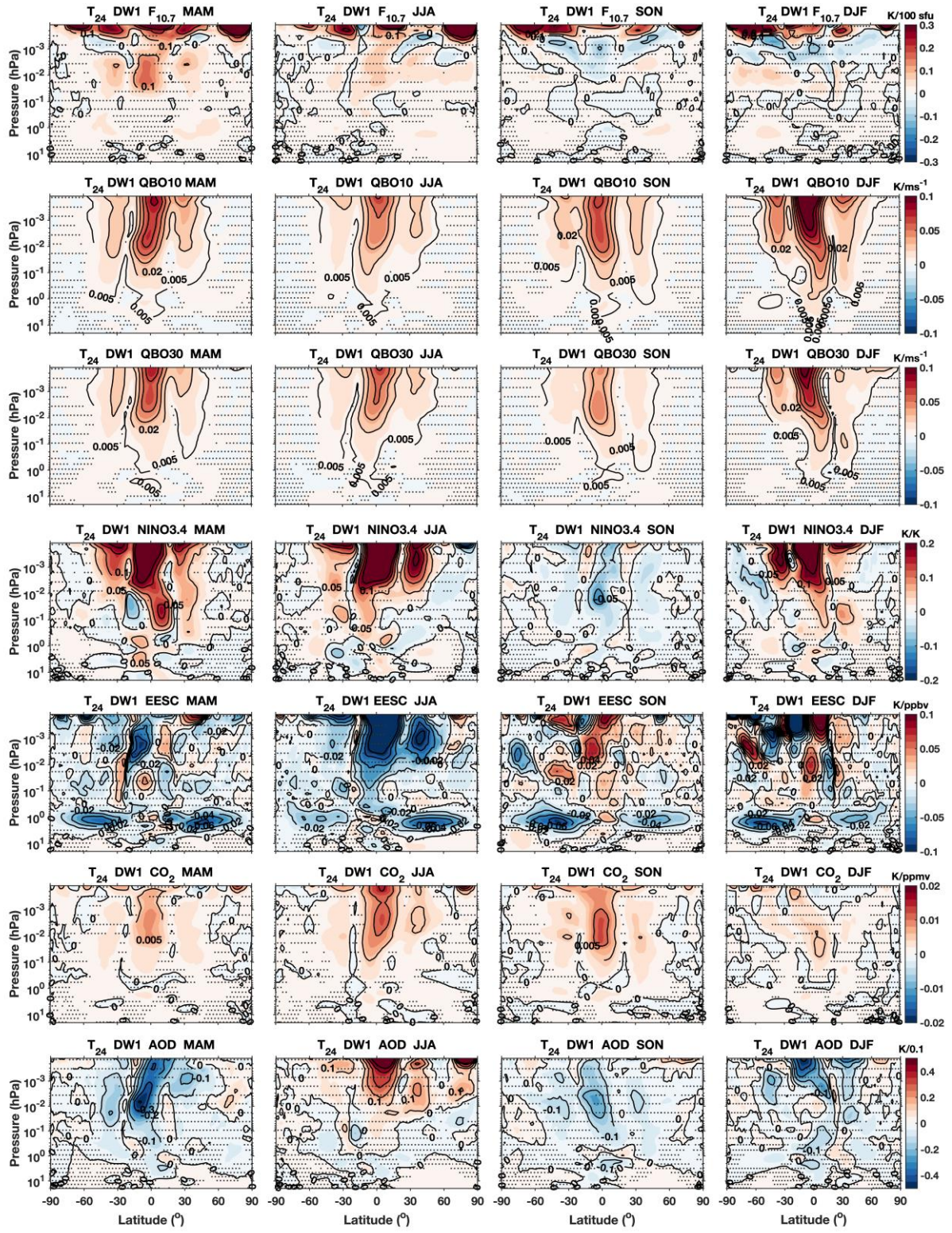

Figure 5. The seasonal variation of latitude-pressure distribution of ΔT_{24} responses to $F_{10.7}$, QBO10, QBO30, NINO3. EESC, CO_2 and AOD averaged for three realizations. The responses in stippled regions are not significant at the 95% confidence level ($p>0.05$). Contour intervals - $F_{10.7}$: 0.1 K/100 sfu, QBO10: 0.015 K/ms^{-1}, QBO30: 0.015 K/ms^{-1}, NINO3.4: 0.05 K/K, EESC: 0.02 K/ppbv, CO_2: 0.005 K/ppmv, AOD: 0.1 K/0.1.

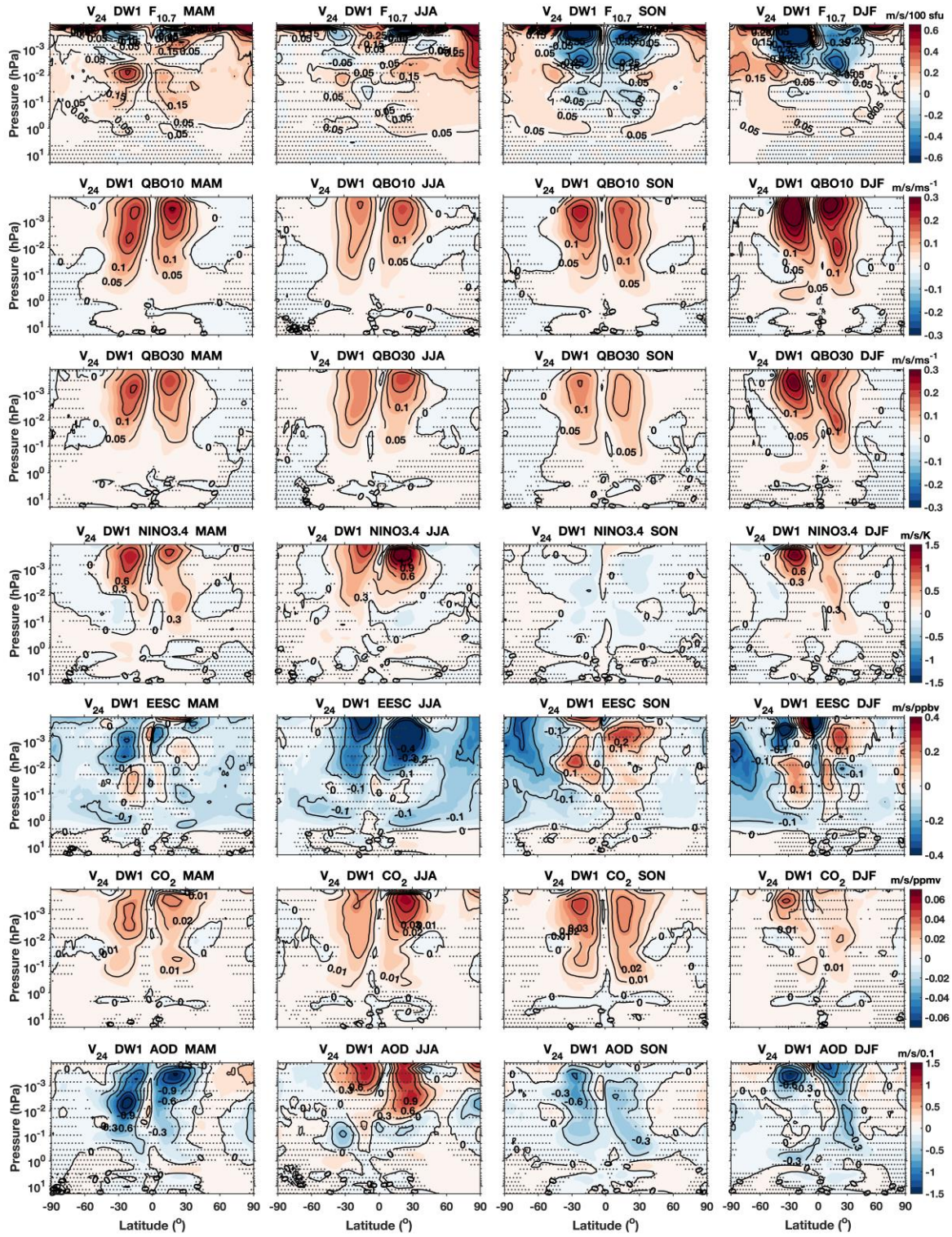

Figure 6. Same as Figure 5 but for ΔV_{24}. Contour intervals - $F_{10.7}$: 0.1 m/s/100 sfu, QBO10: 0.05 m/s/ms^{-1}, QBO30: 0.05 m/s/ms^{-1}, NINO3.4: 0.3 m/s/K, EESC: 0.1 m/s/ppbv, CO_2: 0.01 m/s/ppmv, AOD: 0.3 m/s/0.1.